Eur. J. Mech., B/Fluids, **17,** n° 4, 451–470, 1998

Experimental investigation of turbulence near a large scale vortex

B. ANDREOTTI, J. MAURER, Y. COUDER *, S. DOUADY

ABSTRACT. – The influence of a strong large scale vortex on neighbouring turbulence is investigated. For this purpose the statistical properties of the tangential velocity fluctuations are systematically investigated as a function of the distance to the vortex core. Far from the vortex, the characteristics usually found in isotropic homogeneous turbulence are approximately obtained. In the central region of the vortex a strong decrease of the amplitude of the velocity fluctuations and of the dissipation is observed. However in this region of space the flow is not smooth: the energy spectrum E(k) still exhibits the equivalent of an inertial range but with a slope which can range from $k^{-1.25}$ to k^{-1} instead of the classical $k^{-5/3}$. Furthermore the intermittency is much weaker inside the vortex central region: the velocity differences PDFs no longer exhibit long stretched tails and are more self-similar from scale to scale. In between these two regions, at the periphery of the vortex, the intermittency is strongly increased. It is shown that this increase is due to the mixing in the velocity signal of the two types of statistics (the strongly fluctuating bulk turbulence and the weakly fluctuating vortex flow). This situation is analysed using a variant of extended self similarity that we call LSS (loose self similarity) which lends itself to the analysis of situations where a clear scaling is not obvious. © Elsevier, Paris

1. Introduction

Observing a turbulent flow with anisotropic large-scale structures, it is hard to believe that locally the small scale structures tend to be isotropic even at infinite Reynolds number. The assumed local isotropy in the inertial subrange is somehow linked to the assumption that the interaction is local in Fourier space, so that it is non-local in real space. But, from a hydrodynamics point of view, is it possible that the large and small structures are uncoupled in space? For this reason there have already been many studies on turbulent flows having an anisotropic large scale forcing such as shear driven turbulence or turbulent boundary layers (see for instance Saddoughi and Veeravalli (1994) and references therein). Hitherto no fundamental difference with isotropic turbulence was found in such works and this was a strong support for the hypothesis of the isotropisation of the small scales. However the most coherent structures observed in turbulent flows are vortices so, it may still be worth investigating the influence of the proximity of a large scale vortex on the nature of turbulence in the neighbouring regions. It is well known that a global solid body rotation has a drastic effect on turbulence (Hopfinger *et al.* (1982), Jacquin *et al.* (1990) and Hossain (1993)). Since the central region of a vortex is in fast rotation an effect can be intuitively expected. Characterising a single vortex may reveal a particular signature on the velocity signal which could be recognised in more classical turbulent flows.

We will thus investigate in the present paper the properties of the turbulence near a strong large scale laboratory vortex. This situation is close to the numerical simulation by Melander and Hussain (1993) of the interaction between a strong vortex and a fine scale turbulent background. The work, presented at this conference, by Pinton and Dernoncourt (1997) about turbulence near a precessing vortex is relevant to the same problematic as the present one.

Laboratoire de Physique Statistique, Ecole Normale Supérieure, 24 rue Lhomond, 75231 Paris Cedex 05, France; associé au CNRS et aux Universités Paris VI et Paris VII

* Correspondence and reprints

0997-7546/98/04/© Elsevier, Paris

2. Experimental set-up

Basically the experiment was designed in order to create a strong vortex and to measure the turbulent fluctuations in its vicinity. It is well known that such an isolated vortex is generated in a cylindrical tank if one of the extremities of the cylinder is a rotating disk (see for instance Turner (1966), Escudier (1984), Mory and Spohn (1992)). More recently, we designed a variant of this experiment (Andreotti *et al.* (1997)) where our aim was to investigate the process of vorticity intensification due to the stretching of a single axisymmetric vortex. For this purpose we added the possibility of an axial pumping. We thus demonstrated that when the pump was switched on, it created, at first, a strong longitudinal velocity gradient stretching the vortex. With the increase of the central rotation the bidimensionalisation led to a stationary regime in which the stretching was weakened.

Another geometry providing a swirling flow is that used by Labbé *et al.* (1995) and Chillà *et al.* (1996) where the flow is generated by two corotating disks but is not confined in a cell. In this case, there is formation of a strong vortex whose axis is near the periphery of the disk and which undergoes a slow precessing motion.

In the present work, in order to obtain a stable vortex, we used yet another variant of these experiments in which there are two co-rotating disks located respectively at each extremity of the cylinder and where the fluid is pumped out of the cell through the centre of one of the disks (*Fig.* 1). Wishing to reach high Reynolds number we performed our experiments in low temperature helium gas because of its small kinematic viscosity. Another advantage of using this fluid is that high resolution hot wire detectors can be used to measure the velocity.

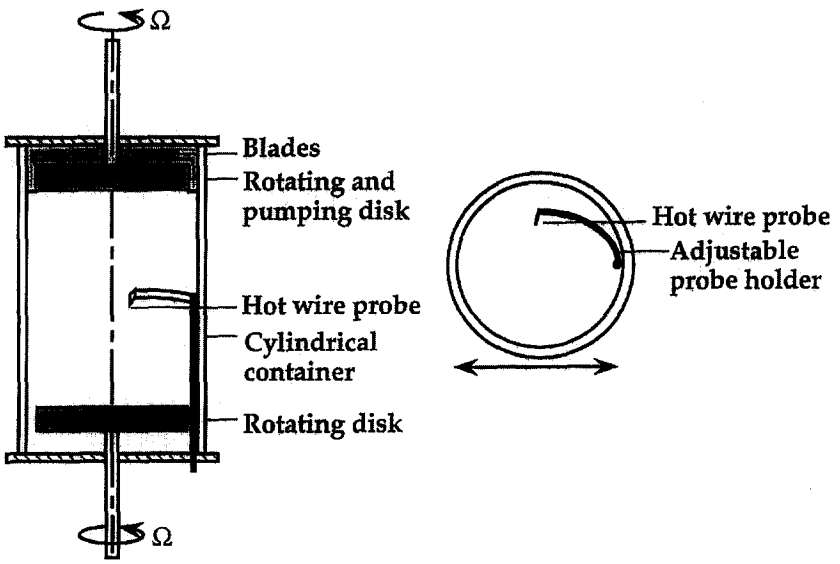

Fig. 1. – (a) A cut of the experimental cell along its axis. (b) A transverse cut of the cell. The probe holder can be rotated on its axis (close to the cylinder) so as to locate the probe at a tunable radial position in the cell.

A problem however is that the best means for the observation of a steady structure remains its direct visualisation. Here the whole experiment being confined in a cryostat there is no possibility of seeing the flow. For this reason we built a second experimental cell exactly homothetic to that used in helium but at a scale 1.5 and filled with water. Using experiments performed in this secondary cell we were able to optimise the design of the pumping disk (see below) and to check that the central vortex survived the disturbance created by the detector holder.

The experimental set-up used for the helium experiment was a variant of that designed by Maurer *et al.* (1994) and Zocchi *et al.* (1994) for their investigation of the dissipation at high Reynolds number. A complete

description can be found in these articles. The cell itself is sketched on Figure 1. The flow is confined in a cylindrical cell of radius R = 38 mm and driven by two coaxial rotating disks placed at each end of the cylinder. The disks are at a distance h = 73 mm from each other. Both disks are set into corotation at frequencies up to 50 Hz by two small dc motors working at low temperature. The first disk (located at the bottom of the cell in *Fig.* 1(a)) is smooth and has a 35 mm radius. The second disk (the top one in *Fig.* 1(a)) has a radius of 28 mm. A hole in the center of the side facing the main flow is connected radially to the periphery of the other side (*Fig.* 1 a). Behind this disk, the rotation is suppressed by six fixed radial blades. This system acts as a centrifugal pump when the disk is rotated. The fluid is sucked out of the cell through the centre of the disk and reinjected in the cell at the disk's periphery.

The fluid velocity is measured with a hot wire probe of a type introduced by Castaing *et al.* (1992) and Zocchi *et al.* (1994). It is made of a 7 μm thick carbon fibre which has a strong variation of its resistivity with temperature in the low temperature range. Most of the length of the fibre is gold plated so that only a length of about 10 μm in its centre is bare and acts as a detector. The fibre being very fragile, it is held on a rectangular frame (6 × 12 mm) made of 250 μm thick steel wire. This frame is then glued onto the extremity of a movable arm (*Fig.* 1 b). This arm is composed of two associated 1 mm thick rods forming a sort of ladder which could be rotated in a plane perpendicular to the cell's axis half way between the disks. A change of position of the detector could be made at will during the experiment, the arm being moved by a small motor working at low temperature.

In all the experiments presented here the hot wire itself is parallel to the cell's axis. We thus record systematically the tangential velocity at regularly spaced radial positions, from the cylinder's wall to the centre. The distance of the detector to the cell's axis being ρ we will report the results using the non dimensional position $r = \rho/R$.

The cell was placed in a liquid helium cryostat and filled with helium gas at T = 4.2 °K and a pressure P = 0.9 Bar so that the gas viscosity was $\nu = 9\ 10^{-4}$ cm^2 s^{-1}. A Reynolds number could be defined as $\mathrm{Re} = \Omega\ \mathrm{R}^2/\nu$ where Ω is the angular velocity of the disks. The present experiments, performed at $\Omega = 240$ s^{-1}, correspond to a Reynolds number $\mathrm{Re} \sim 3.5\ 10^6$. We can remark that with such an inhomogeneous flow as investigated here this Reynolds number does not have much meaning and we will rather use a local Re_λ based on the measurements of the local Taylor microscale λ.

The detector was calibrated using King's law. The data was digitised by a 16 bit converter controlled by a digital signal processing. The sampling rate was chosen so that no relevant part of the spectrum was left out. Most recordings were done with a 125 kHz rate. With an acquisition time of 10 minutes this meant files of $7.5\ 10^7$ points.

3. Statistical properties of the velocity signal

3.1. Large scale structure of the flow, global observations

The experiment performed in water, reaching a Reynolds number $\mathrm{Re}_{\mathrm{Water}} \sim 5\ 10^5$ was a useful model to observe the global structure of the flow. While it is always characterised by a strong central vortex, this vortex can be either stable or unstable, exhibiting in this case vortex breakdowns. The strength of the pumping was chosen to that the vortex would be stable enough to resist the disturbances due to the model detector holder to a certain extent.

We use both kalliroscope and air bubbles to inspect the structure of the flow in the absence of the detector. When a laser light plane cuts through the cell it is clear that the flow in the outer region has much larger turbulent fluctuations. In a central column of radius approximately 1.5 cm ($r \sim 0.5$) the 3 D fluctuations are

seen as much weaker. In the presence of bubbles, they mark the axis of the vortex so that its position is easily observed: it appears as stable and approximately fixed. When the arm carrying the detector moves, the flow is at first only slightly disturbed. However when it reaches about $r \sim 0.3$ the disturbances become stronger. The region of weakened 3 D fluctuation is then limited roughly by the probe position, and the vortex starts vibrating. Paradoxically the disturbance appears somewhat weaker when the probe is at the cell's centre: the vortex is slightly pushed away from the detector and still vibrates but this global motion now has a small amplitude.

For these reasons, the measurements presented below do not strictly correspond to a cut through an undisturbed system. Each position of the probe changes the geometrical configuration of the flow. In particular, we probably never reach the axis of the vortex with the detector. But the visual observation as well as the experimental results are sufficient to demonstrate that for all positions of the probe, there exist a strong central vortex and that when $r \leq 0.2$ the detector is located within the central region of this vortex.

All the experiments in helium reported here were performed with the two disks rotating at the same angular velocity $\Omega = 240$ s^{-1}. The velocity signal was recorded systematically at different probe positions r. From these velocity recordings, we computed the radial profile of the mean tangential velocity U and that of the root mean square of the velocity fluctuations $u'_{\rm rms}$. Both profiles are given on Figure 2 a. They show that the flow is inhomogeneous in space. Starting from the cell's periphery ($r = 1$) and approaching the centre, the mean velocity first increases because of the presence of the vortex, then decreases when entering the central region. This decrease is due both to the intrinsic velocity profile inside the vortex and to the influence of the probe holder. Simultaneously $u'_{\rm rms}$ can be seen to decrease. We can also note that the ratio $u'_{\rm rms}/U$ is relatively large ($\sim$ 40%) at the periphery. This is a common feature of the turbulent experiments performed in closed cells (e.g. Zocchi *et al.* (1994)). With this high fluctuation it is still possible to use a Taylor hypothesis but a precise analysis would require the use of the correction introduced by Pinton and Labbé (1994). This was not done here since we are mainly interested in the central region were the fluctuations are sufficiently small, $u'_{\rm rms}/U \sim 6\%$, for the Taylor hypothesis to be used.

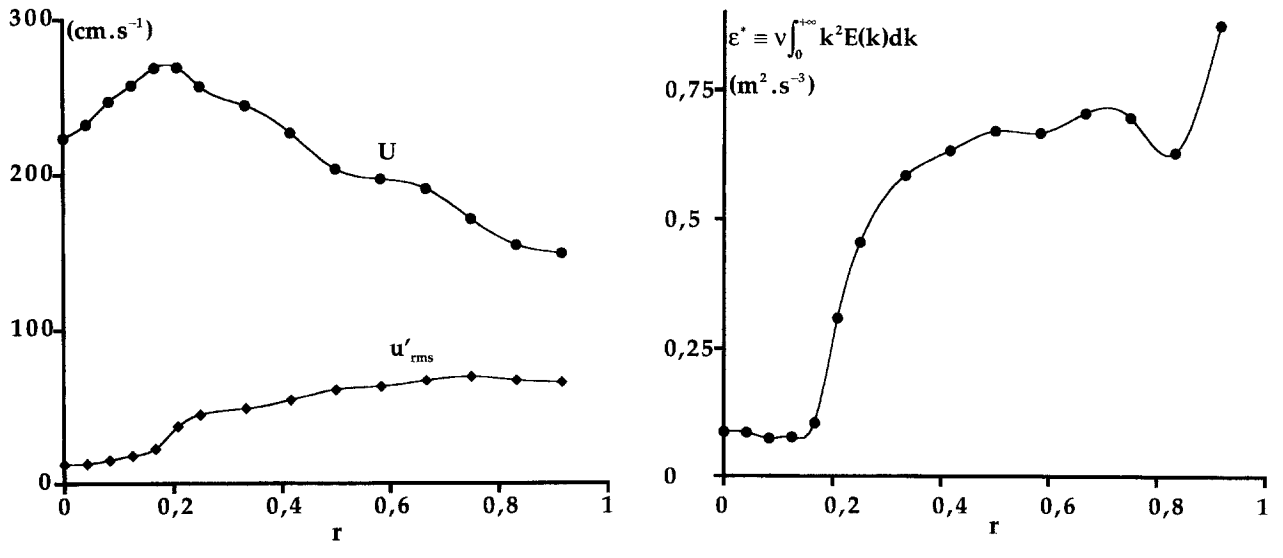

Fig. 2. – (a) Evolution of the mean velocity U (Black dots) and of the fluctuation velocity $u'_{\rm rms}$ as a function of the non dimensional radial position r of the probe. (b) Radical evolution of the "dissipation rate" ε^*.

Another problem could arise with this type of closed flow for large time increments. Indeed, if the streamlines of the mean flow U are closed lines, the fluctuations on the probe at a given time, and one turnover time later, are the same (under the frozen turbulence assumption). Length scales larger than the length of this closed streamline would have no sense. However, no strong large scale self correlation of the velocity signal is observed. As a consequence, a given region which passes in front of the probe must either rarely pass a second time (in the case of spirals streamlines for instance) or undergoes a lot of change in one turnover time. As the fluctuation rate is small, the frozen turbulence hypothesis is valid, so the streamlines are mainly spirals. In what follows, the scales larger than one turn around the vortex will also be plotted. One should thus keep in mind that the increments are not taken on a straight line but on mean streamlines which are curved.

The inhomogeneity of the flow is confirmed if we compute the one dimensional approximation of the mean dissipation rate ε^*. Since we are far from the isotropic case we do not introduce any prefactor and thus prefer to introduce this pseudo dissipation ε^* as:

$$\varepsilon^* \equiv \nu \int_0^\infty k^2 E(k) dk \tag{1}$$

It must be noted that in the case of a homogeneous and isotropic Kolmogorov turbulence, the dissipation rate ε is $\varepsilon = 15\,\varepsilon^*$. The computed value of ε^* as a function of the position in the cell is plotted in Figure 2 b. It is almost constant in the outer region (for $r > 0.4$, $\varepsilon^* \approx 0.68$ m$^2 \cdot$ s^{-3}) and in the inner region (for $r < 0.3$, $\varepsilon^* \approx 0.08$ m$^2 \cdot$ s^{-3}). The strong decrease between these two values is localised in a thin region which corresponds to $0.3 < r < 0.4$. Note that the variation of $u'_{\rm rms}$ and ε^* are very similar. This means that the reduction of the fluctuations is observed both on the large scales ($u'_{\rm rms}$) and on the small scales (ε^*).

Based on these two quantities, we can classically construct the Taylor microscale by:

$$\lambda = u'_{\rm rms} \left(\int_0^\infty k^2 E(k)\, dk \right)^{-1/2} \tag{2}$$

so that the microscale Reynolds number is

$$\mathrm{Re}_\lambda = \frac{u'_{\rm rms}\,\lambda}{\nu} \tag{3}$$

At the velocities used in the present experiment it varies from $\mathrm{Re}_\lambda \sim 1900$ at the periphery to $\mathrm{Re}_\lambda \sim 300$ in the central region. Finally the Kolmogorov scale

$$\eta = (\nu^3/\varepsilon)^{1/4} \tag{4}$$

will be used when possible.

We found that the statistical properties of the signal are functions of the radial position as the mean properties of the flow. This is obvious by direct observation of the velocity time series. Three randomly chosen samples of velocity fluctuation are shown on Figure 3. In the outer region of the cell ($r = \rho$, $R_0 > 0.5$), an apparently normal turbulent signal is observed with large amplitude fluctuations (*Fig.* 3 a). Inside the vortex core, near the cell's centre ($r < 0.2$), the signal also seems to be a normal turbulent signal but with a strongly reduced fluctuations amplitude (*Fig.* 3 c). Finally, in an intermediate region at the periphery of the vortex ($0.2 \leq r \leq 0.5$) the signal is very intermittent and shows weak fluctuations interrupted by strong (relatively negative) velocity peaks (*Fig.* 3 b).

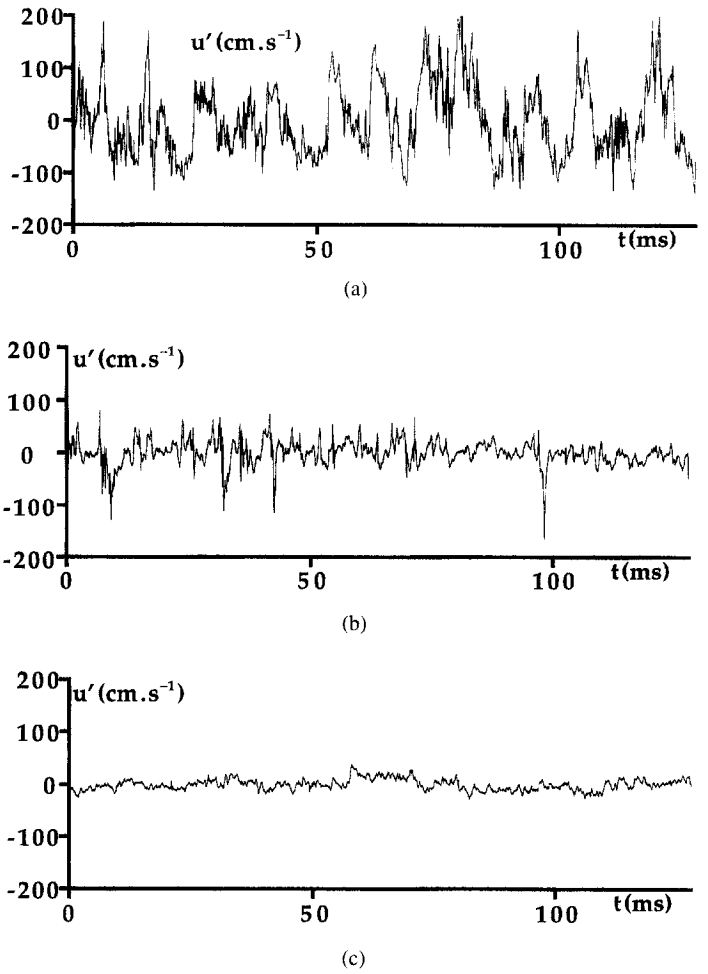

Fig. 3. – Three recordings of the velocity as a function of time. (a) Recording in the external part of the cell (at $r = 0.75$). (b) Recording at the periphery of the vortex central region (at $r = 0.2$). (c) Recording in the central region (at $r = 0$).

3.2. On scaling exponents

In the following we will report separately the statistical analysis of the signal and particularly of its intermittency in each of these three regions. For this purpose, we will first give the probability density functions of the velocity differences $P_l(\delta u')$ for various interval scales. These PDFs are estimated from the experimental histograms of the velocity increments, using a regularisation method. This technique allows a precise estimation of the PDF up to the last point of measurement (the rarest event). Details about this method, its tests on synthetic signals and its application to turbulence may be found in Andreotti and Douady (1997).

Then we will examine the scaling of the structure functions.

$$S_p(l) = \langle [u'(t) - u'(t + l/U)]^p \rangle \tag{5}$$

In classical experiments, $S_p(l)$ scales in the inertial range as a power of l:

$$\ln [S_p(l)] \approx \zeta_p \ln(l) + c^{st} \tag{6}$$

The deviation of ζ_p from the value $\zeta_p = p/3$ predicted by Kolmogorov in 1941 is often thought of as characterising the intermittency. But strictly speaking the intermittency corresponds to the existence of rare events of strong velocity differences and thus to the presence of tails in the velocity differences PDFs. As for the scaling exponents ζ_p they are a measure of how the PDFs change with the interval scales. The deviation of the ζ_p from $p/3$ is not a characteristic of the intermittency but a characteristic of the increase of the intermittency at small scales.

Benzi *et al.* (1993) have demonstrated that better scaling properties are obtained when the moments are expressed as a function of the third order moment.

$$\ln [S_p (l)] \approx \zeta_p^* \ln [S_3 (l)] + c^{st} \tag{7}$$

In the case where both exist, the direct and relative exponents are related by $\zeta_p^* = \zeta_p/\zeta_3$. In the hypothesis of an isotropic homogeneous turbulence, the third exponent ζ_3' (computed without absolute value) is equal to one. It is often assumed that the exponent computed with absolute value ζ_3 is the same. When this is true, the direct exponents ζ_p and the ESS ones ζ_p^* are equal. However, it must be underlined that the relative exponents ζ_p^* can often be computed when the ζ_p cannot be defined or when ζ_3 is not equal to one. For this reason this method, usually called Extended self similarity (ESS), should, in our opinion, rather be called relative self similarity.

We will also use a new version of the Extended Self Similarity which we express by the relation:

$$[(p-1) \ln [S_p (l)]] \approx \zeta_p^{**} [p \ln (S_{p-1} (l))] + c^{st} \tag{8}$$

From a theoretical point of view, this is just another version of ESS because for a really self-similar signal the set of relative exponents ζ_p^{**} is strictly equivalent to the set of usual ESS exponents ζ_p^*. If there really exists a range where the power law of equation (8) is strictly correct, ESS (equation (7)) will also be valid. In this case the relation between the two types of exponents is:

$$\zeta_p^{**} = \frac{p}{p-1} \frac{\zeta_p^*}{\zeta_{p-1}^*} \tag{9}$$

For perfectly self similar signals all the $\zeta_p^{**} = 1$.

The reason for the introduction of these exponents is that from a pragmatic point of view, the usual ESS plots often exhibit distortions which increase when p increases. The new log-log plots of $S_p (S_{p-1})$ are straighter than those of ESS because the distortions are spread amongst the successive orders. The change between the shapes of $S_p (l)$ and $S_{p-1} (l)$ being generally continuous and small, exponents ζ_p^{**} can be defined and measured even when ESS fails. The danger is that this means that with this method it is possible to obtain ζ_p^{**}, even when there is no real scaling behaviour. In such cases the ζ_p^{**} are not, strictly speaking, exponents. For this reason we chose to call this method the loose self similarity (LSS). However, we will use it, because the ζ_p^{**} give quantitative information on the PDF evolution.

A particular model of intermittency has been proposed by Dubrulle (1994). The turbulence signal is assumed to be log-Poisson. This gives a general expression for the values of the ESS exponents:

$$\zeta_p^* = (1-\Delta) \frac{p}{3} + \frac{\Delta}{1-\beta} (1 - \beta^{p/3}) \tag{10}$$

It is a generalisation of a previous theory due to She and Lévêque (1994) who proposed a physical interpretation of the parameters Δ and β. The first parameter Δ is related to the codimension of the most

intermittent structures, and the second β is linked to the degree of intermittency. In the case of homogeneous and isotropic turbulence, the more intermittent structures are assumed to be vorticity filaments, and this fixes the parameters values to $\Delta = \beta = 2/3$ with also $\zeta_3 = 1$ so that:

$$\zeta_p = \frac{p}{9} + 2\left[1 - \left(\frac{2}{3}\right)^{p/3}\right] \tag{11}$$

Expression (11) gives a good fit to the values obtained experimentally in various classical turbulence experiments.

3.3. Results far from the vortex

In the region $r \geq 0.5$, the characteristics of turbulence are close to usual. For $r = 0.7$, the Taylor scale Reynolds number Re_λ is 1900. The energy spectrum obtained for $r = 0.7$ is shown on Figure 4. It exhibits on more than a decade a slope of – 1.7, close to the classical – 5/3 value shown for comparison. Figure 5 shows the PDFs of the velocity increments for length scales 1 of respectively 8 10^{-3}, 6 10^{-2}, 5 10^{-1} and 4 mm. Each of them is normalised by its standard deviation σ_1. The Kolmogorov scale can be determined and is $\eta = 3$ μm so that the above lengths correspond approximately to 2.7 η, 20 η, 166 η, 1333 η. The PDFs exhibit a classical quasi-Gaussian behaviour at large scales, and long tails at small scales. The small scale intermittency is due to rare events. In order to get an order of magnitude we can note that in the dissipative range with a probability 10^{-7} the rare events are as large as 22 times the standard deviation.

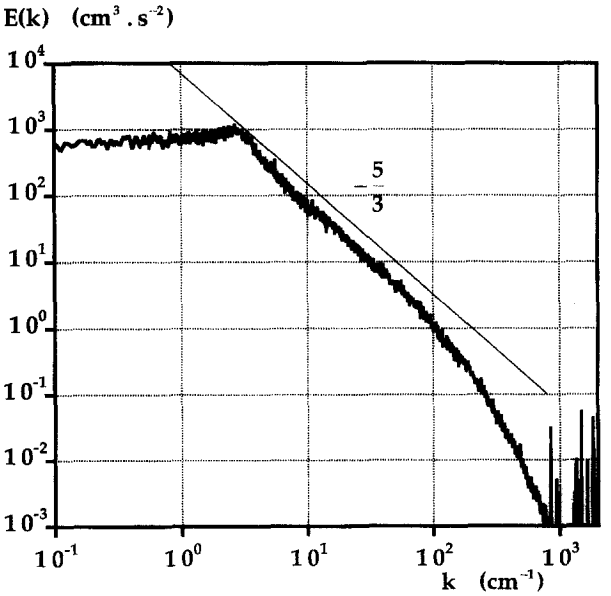

Fig. 4. – *External region of the cell.* The energy spectrum obtained at $r = 0.75$. The full line corresponds to the Kolmogorov slope – 5/3.

Finally we determine the exponents of the structure function. The plot of $\mathrm{Log}\,(S_p\,(l))$ as a function of $\mathrm{Log}\,(l)$ shows a range of scaling of approximately one decade and a half. This is observed for instance on *Figure* 6, which shows $\mathrm{Log}\,(S_6\,(l))$ as functions of $\mathrm{Log}\,l$. The best fit of the linear region provides the value of the scaling exponent ζ_p. The third exponent of the structure function ζ_3 is around 1.07 while a value of 1 was expected. The scaling behaviour is somewhat better on the plot of $\mathrm{Log}\,(S_6\,(l))$ as a function of $\mathrm{Log}\,(S_3\,(l))$

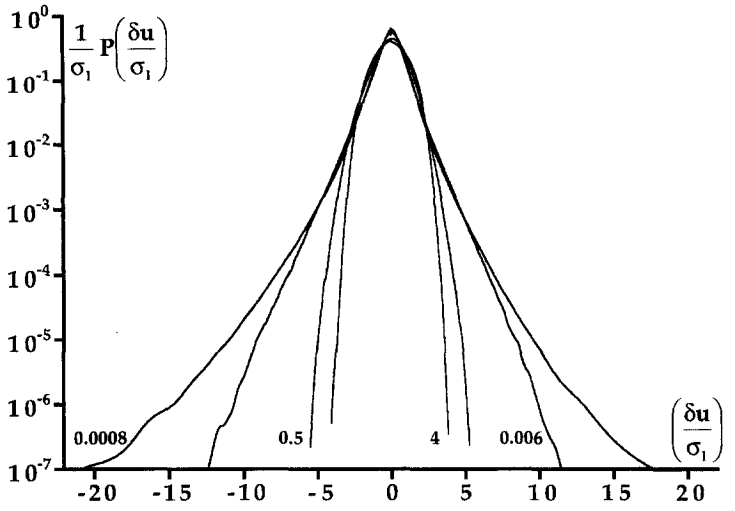

Fig. 5. – *External region of the cell.* Four velocity increments probability distribution functions renormalised with their standard deviation for length scales of respectively 8 10^{-3}, 6 10^{-2}, 5 10^{-1} and 4 mm. The Kolmogorov scale is $\eta = 3\ \mu m$.

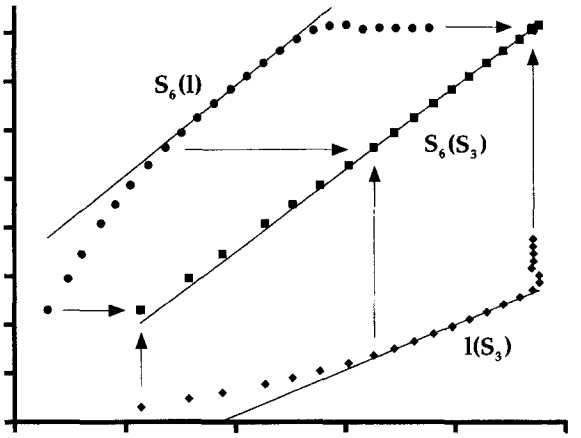

Fig. 6. – *External region of the cell.* Determination of the exponents of the structure functions. Black dots: Log $(S_6\,(l))$ as a function of Log (l). The fitting line has slope ζ_6. Black diamonds: Log (l) as a function of Log $(S_3\,(l))$. Black squares: Log $(S_6\,(l))$ as a function of Log $(S_3\,(l))$. The fitting line has slope ζ_6^*. The three curves are plotted simultaneously to show how ESS flattens the structure function variations.

shown on Figure 6. The linear collapse due to ESS is well understood if the plot $S_6\,(l)$ is related to the plot of $l\,(S_3)$ as can be seen on Figure 6.

Similar plots were done for various p and the exponents were deduced from the corresponding slopes. The values obtained for ζ_p and ζ_p^* are summarised on Figure 7 and Table 1. The values of ζ_p are very close to the values found for most recent experiments (Arneodo *et al.* (1996)) (dashed line on *Fig.* 7). It is worth noting that when ESS is used, the relative exponent ζ_3^* is set to one by definition. This is the major source of the difference between ζ_p and ζ_p^* observed in Figure 7. If the curve for ζ_p^* is further shifted from the self-similar $(p/3)$ straight line, this is only because ζ_3 is larger than one. The ζ_p^* curve can be fitted by the Log Poisson model of equation (10) (She-Lévêque (1994) and Dubrulle (1994)). The parameters obtained are: $\Delta = 0.83$ and $\beta = 0.64$. The value for Δ, related to the codimension of the most intermittent structures, is here larger than

the 2/3 predicted in She-Lévêque model. The second parameter β, linked to the degree of intermittency, is of the same order as the predicted 2/3.

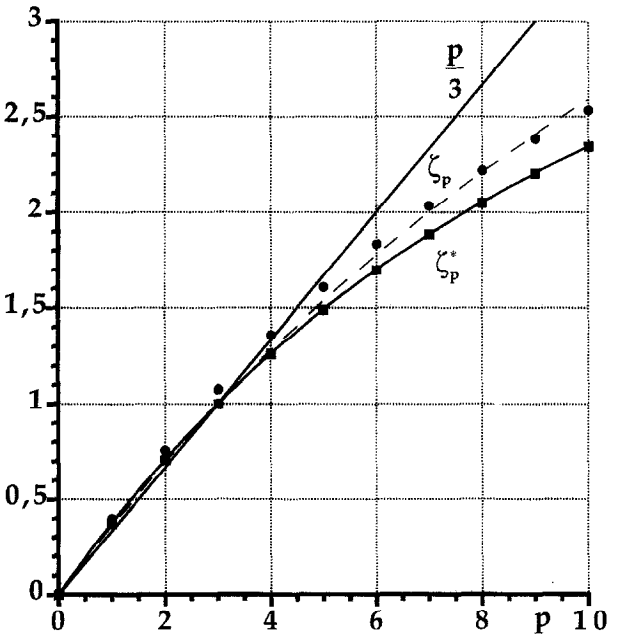

Fig. 7. – *External region of the cell.* Exponents of the structure functions: the ζ_p are the values obtained directly and ζ_p^* those obtained using ESS. The dashed line shows the values usually found in homogeneous turbulence.

TABLE I. – Comparison of the structure functions exponents as functions of their order p, for the following cases: as predicted by K41, by the She-Lévêque model (Eq. 11), and as measured in the three regions of the experiment, both directly and using ESS (with $\zeta_3^* = 1$). (For the unknown author who says "In science, one has to turn to numbers").

	K41	S-L	Outer region		Vortex Centre		Intermediate Region	
p	ζ_p	ζ_p	ζ_p	ζ_p^*	ζ_p	ζ_p^*	ζ_p	ζ_p^*
0	0.00	0.00	0.00	0.00	0.00	0.00	0.00	0.00
1	0.33	0.36	0.40	0.37	0.21	0.34	0.41	0.51
2	0.67	0.70	0.76	0.71	0.42	0.68	0.68	0.83
3	1.00	1.00	1.07	1.00	0.62	1.00	0.85	1.00
4	1.33	1.28	1.36	1.26	0.82	1.31	0.96	1.13
5	1.67	1.54	1.61	1.49	1.00	1.61	1.07	1.26
6	2.00	1.78	1.83	1.70	1.18	1.89	1.19	1.40
7	2.33	2.00	2.04	1.88	1.34	2.16	1.31	1.54
8	2.67	2.21	2.22	2.05	1.49	2.39	1.43	1.68
9	3.00	2.41	2.39	2.20	1.60	2.57	1.54	1.80
10	3.33	2.59	2.54	2.34	1.65	2.65	1.64	1.92

3.4. CLOSE TO THE CELL'S AXIS

Close to the cell's axis the probe is, as stated above, in the vortex central region. However, the vortex being pushed by the probe holder, the measurement point is not on the axis of the vortex but as near as possible to this axis. Indeed, as shown on Figure 2, the mean velocity U is still very large at this position. As stated above, the

fluctuating velocity signal has a reduced amplitude. More remarkable is the fact that the energy spectrum itself is, in this region, completely different from Kolmogorov's type. Figure 8 shows that there is a kind of inertial range but where the slope is approximately equal to – 1.17. It is followed at large k by a kind of dissipative range. Note however that this decrease is straighter, with a larger slope (around – 3), and a sharper transition than the usual viscous cut off. It is worth noting that other spectra recorded moving inward have well defined slopes increasing from – 1.25 to – 1.05. Compared to the spectrum observed far from the centre, the signal appears less rough in amplitude, but with a stronger roughness exponent.

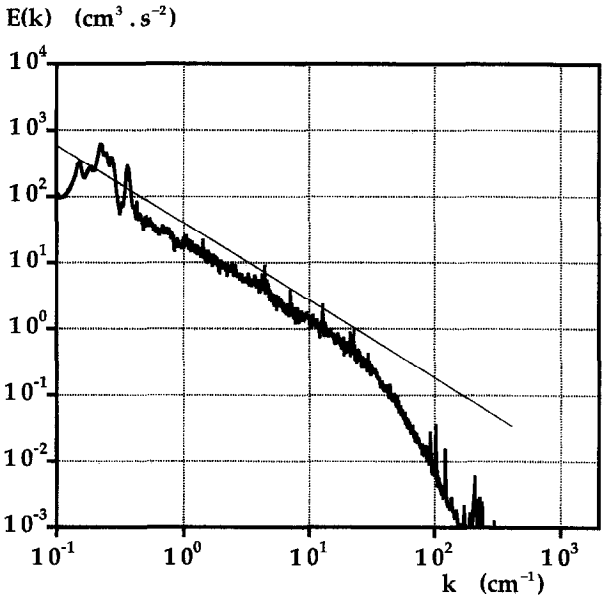

Fig. 8. – *Centre of the cell.* The energy spectrum obtained at $r = 0$. The full line corresponds to the best fit slope – 1.17.

The velocity increments PDFs are also very different, as shown on Figure 9. They all appear to be nearly Gaussian for the small velocity differences and to have very weak exponential tails. Compared to the usual turbulence PDFs, they appear much more self similar from scale to scale. Thus, the intermittency is reduced in the sense that the small scale PDFs exhibit a reduced tail. At the smallest scale (in the dissipative range) the rare events having a probability 10^{-7} are only of the order of 13 times the standard deviation, thus having an amplitude 0.6 times that obtained in the previous PDFs.

This weak intermittency was also characterized by the measurements of the exponents of the structure function. The plots of $\mathrm{Log}\,(S_p\,(l))$ as a function of $\mathrm{Log}\,(l)$ do not show a well defined scaling (*Fig.* 10). We thus compared the values of the ζ_p on a common range of scales shown in Figure 10. The resulting exponents are very different (*Fig.* 11 and Table 1) from the usual values. They appear close to a linear dependence: $\zeta_p \approx 0.2\,p$. In particular, $\zeta_3 = 0.62$ instead of 1 as predicted in the case of a homogeneous and isotropic flow. These results are coherent with the differences of the spectrum slopes. It is still possible to use the Extended Self Similarity technique, knowing however that the reference exponent ζ_3 does not have the usual meaning. Figure 10 shows that when $\mathrm{Log}\,(S_6\,(l))$ is plotted as a function of $\mathrm{Log}\,(S_3\,(l))$ a relatively good scaling reappears. For the sake of comparison with the previous data it is possible to plot the relative slopes ζ_p^*. When this is done (*Fig.* 11 and Table 1) the values of ζ_p^* appear nearer than usual to the self similar $p/3$ line, the signal thus being less intermittent.

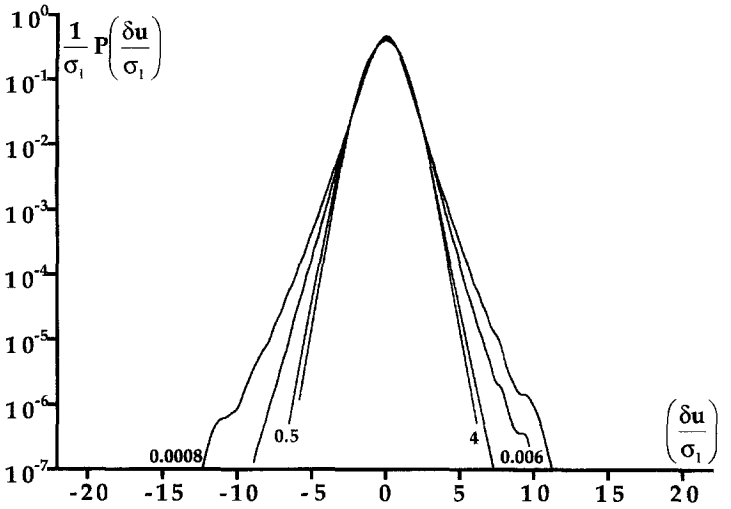

Fig. 9. – *Centre of the cell.* Four velocity increments probability distribution functions renormalised with their standard deviation for length scales of respectively 8 10^{-3}, 6 10^{-2}, 5 10^{-1} and 4 mm.

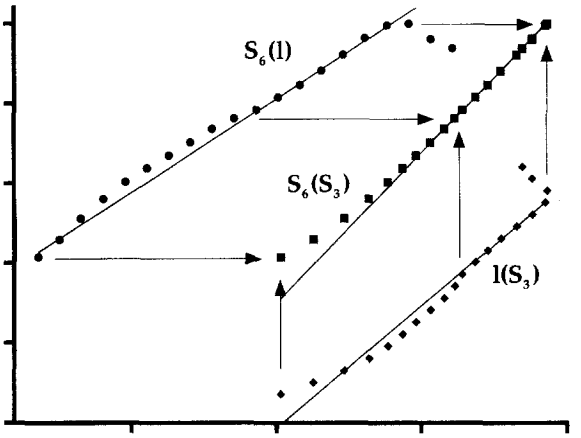

Fig. 10. – *Centre of the cell.* Determination of the exponents of the structure functions. Black dots: $\mathrm{Log}\,(S_6\,(l))$ as a function of $\mathrm{Log}\,(l)$. The fitting line has slope ζ_6. Black diamonds: $\mathrm{Log}\,(l)$ as a function of $\mathrm{Log}\,(S_3\,(l))$. Black squares: $\mathrm{Log}\,(S_6\,(l))$ as a function of $\mathrm{Log}\,(S_3\,(l))$. The fitting line has slope ζ_6^*.

This self-similarity is in fact the reason why the generalised extended self-similarity (GESS) was not used. This other extension of ESS is defined by:

$$[\ln(S_p(l)) - p/3\ln(S_3(l))] \approx \zeta_{pq}^{***}\,[\ln(S_q(l)) - q/3\ln(S_3(l))] + c^{st} \tag{12}$$

The non dimensionalisation of the two terms leads to the subtraction of the regular self-similar part of the signal. In the case of a perfectly self-similar signal, this definition is not well defined: each curve collapses into a single point, and it is difficult to deduce a slope from a single point. With the signal obtained here in the vortex core, we did not get a point but a noisy scatter plot on a small region. As GESS was useless in this case, we did not use it in the other cases either. A practical remark is also that the structure function exponents are not very sensitive measurements. It is more instructive to work directly on the energy spectrum and rescaled PDF. Comparing the results obtained in the core region and in the outer region, the structure function exponents

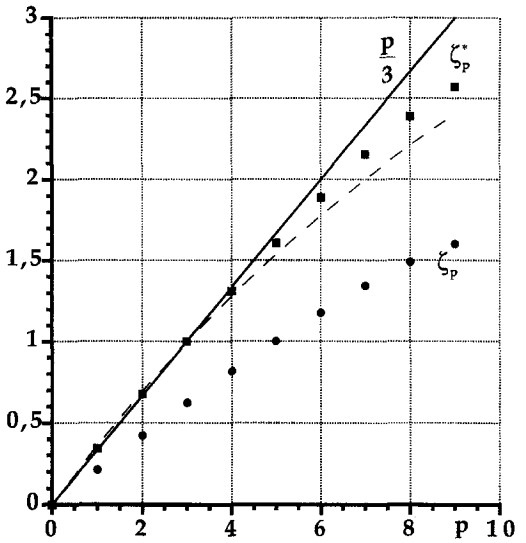

Fig. 11. – *Centre of the cell.* Exponents of the structure functions: the ζ_p are the values obtained directly and ζ_p^* those obtained using ESS. The dashed line shows the values usually found in homogeneous turbulence.

curves are rather close (*Fig.* 7 and 11), however the differences on the energy spectra and even more on the rescaled PDFs are visible at first sight (*Fig.* 4 and *Fig.* 8, *Fig.* 5 and *Fig.* 9).

3.5. Around the vortex

The velocity signal is more complex at the periphery of the vortex central region. In particular it presents strong intermittent peaks (*Fig.* 3 b). The spectrum (*Fig.* 12) exhibits no clear global scaling. In particular two broad band frequency peaks can be distinguished. They can be tentatively associated to the wake generated by the detector holder.

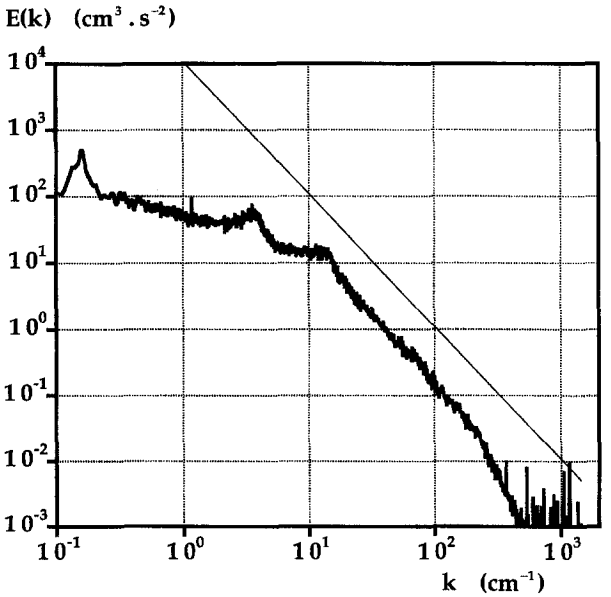

Fig. 12. – *Boundary of the vortex central region.*
The energy spectrum obtained at $r = 0.2$. The full line has a slope – 2.

Looking now at the velocity increments PDFs (*Fig.* 13), the only one to be approximately normal is at the largest scale. The others clearly appear as the superposition of high probability weak fluctuations and of rarer fluctuations with a much larger amplitude. Moving the probe towards the centre the large amplitude fluctuations become more and more rare. There is a continuous decrease of the PDFs tails and a correlated growth of the central bump.

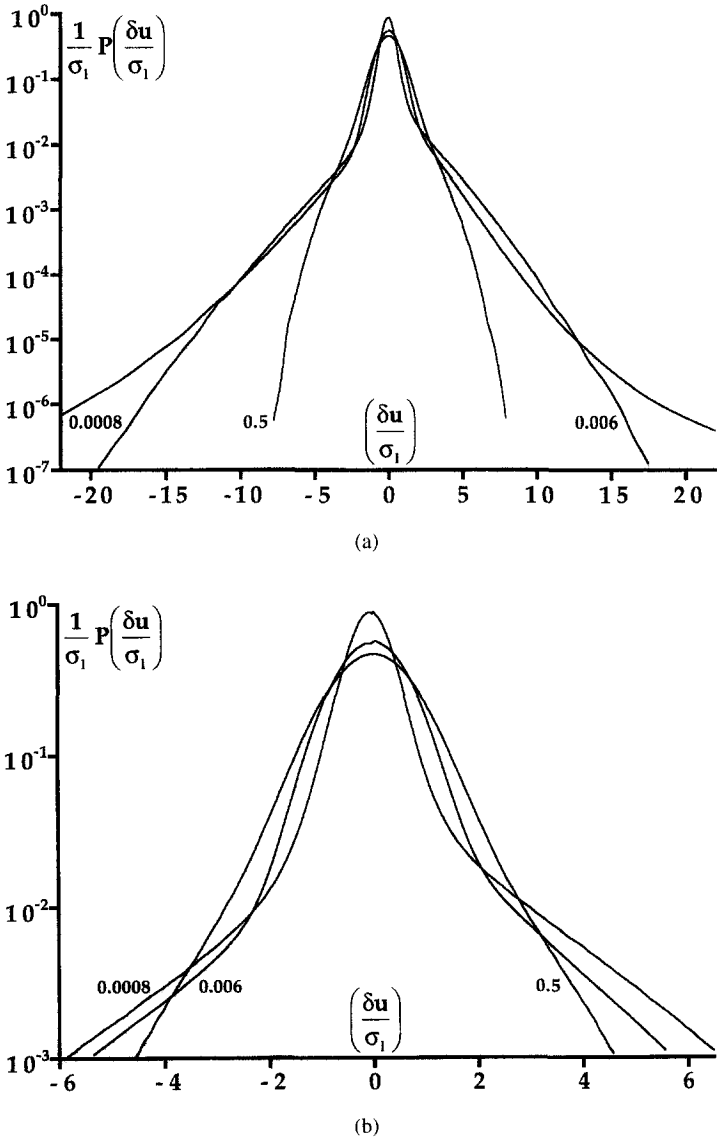

Fig. 13. – *Boundary of the vortex central region.* (a) Four velocity increments probability distribution functions renormalised with their standard deviation for length scales of respectively 8 10^{-3}, 6 10^{-2}, 5 10^{-1} and 4 mm. (b) Close-up of the central region of the PDFs.

These characteristics are easy to understand with the help of the visualisation in water. In this region we can see that the vortex undergoes an irregular global motion so that the probe gets in and out of the vortex central region. As a consequence, the signal's statistical properties present both the character of the "vortex core turbulence" and that of the "outer region turbulence". It can be seen on the velocity signal (*Fig.* 3 (b)) that

the alternance of the signal of type "vortex" and of type "outer region" can be rapid. The signal is composed of domains of large average velocity but small fluctuations and other domains of weaker average velocity but large fluctuations. The former correspond to the small amplitude of the fluctuations in the central region, the latter to the smaller U and larger fluctuations u' outside this region.

The velocity differences PDFs (*Fig.* 13 (b)) also clearly reveals this mixing. At small scale (8 μm), the velocity increment PDF can be seen as the weighted sum of two functions, the rarest events i.e. the PDF tail corresponding to the "outer region" statistics and the most probable events to the "vortex central region" statistics. The crossover between these two functions appears very sharp for this scale. When the length scale of the increment increases, this crossover becomes more and more smooth and the statistics more and more convoluted with one another.

This large scale smoothing effect can be interpreted simply. Let us consider a particular velocity increment $u'(x+l/2) - u'(x-l/2)$ in the signal and call $(x-l/2)$ the left point of the increment and $(x+l/2)$ its right point. At small scale, there is a strong probability to get both the left and right points in a "vortex central region" or in a "outer region". When the scale increases, there are more and more increments which have the left point governed by one type of statistics and the right point governed by the other limit statistics. This induces a regularisation of the cut-off when the scale of the increments becomes of the order of the typical sizes of the homogeneous regions.

In spite of this mixture it is still interesting to see whether the scaling exponents provide some information in this complex situation. The plots of $\mathrm{Log}\,(S_p\,(l))$ as a function of $\mathrm{Log}\,(l)$ do not show any clear scaling. The only thing which can be done to compute a value of ζ_p is to measure the tangent to these curves on the half decade where these plots are rather straight. Finally, when ESS is used, the collapse of the points at large scale plots slightly increases the degree of scaling so that values of ζ_p^* can be computed with reasonable error bars. Once plotted on Figure 15 the values of ζ_p and ζ_p^* exhibit a very strong deviation from the $p/3$ self-similar behaviour. This means that the coexistence of two different types of signals, one of strong amplitude with quite strong intermittency (outer region) and one of small amplitude with weak intermittency (vortex core) results in a strong enhancement of the global intermittency. To give an order of magnitude, the rare events having a probability 10^{-7} are here more than 30 times the standard deviation. This strong effect can be simply interpreted as an increase of the contrast between the most probable fluctuations and the rare ones. The crossover in the velocity

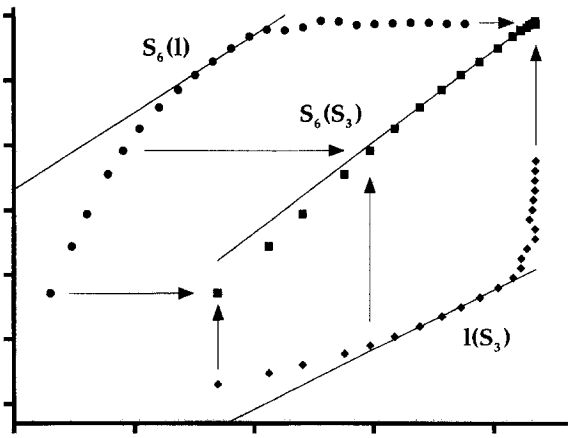

Fig. 14. – *Boundary of the vortex central region.* Determination of the exponents of the structure functions. Black dots: $\mathrm{Log}\,(S_6\,(l))$ as a function of $\mathrm{Log}\,(l)$. The fitting line has slope ζ_6. Black diamonds: $\mathrm{Log}\,(l)$ as a function of $\mathrm{Log}\,(S_3\,(l))$. Black squares: $\mathrm{Log}\,(S_6\,(l))$ as a function of $\mathrm{Log}\,(S_3\,(l))$. The fitting line has slope ζ_6^*. Again, the three curves are plotted simultaneously to show how ESS flattens the structure function variations.

increments PDFs between the two signals appears for the scaling exponents around $p = 3$. This correspond to a rupture in the curve, from a first part close to $p/3$ to a second one surprisingly straight with a much smaller slope. The observed asymptotic slope is 0.11 for the direct exponents and 0.133 for the relative ones. It is worth noting that 0.11 is approximately equal to 1/9 which is the asymptotic slope predicted for normal turbulence by the She Lévêque model when p tends to infinity (relation (11)).

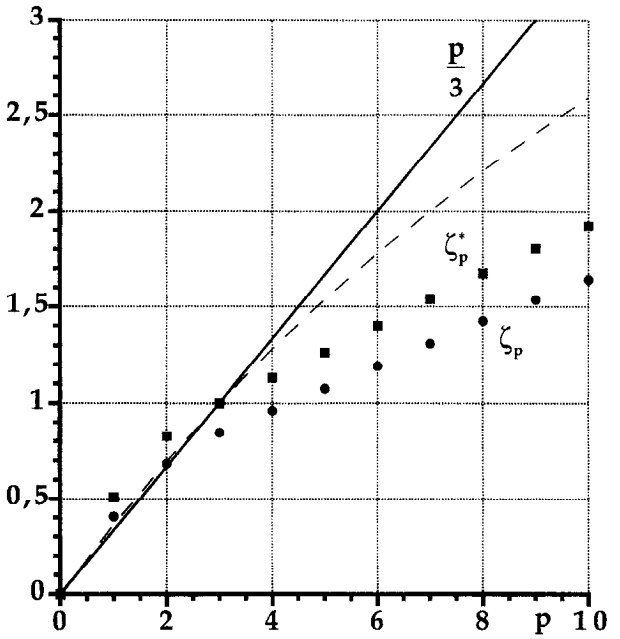

Fig. 15. – *Boundary of the vortex central region.* Exponents of the structure functions: the ζ_p are the values obtained directly and ζ_p^* those obtained using ESS. The dashed line shows the values usually found in homogeneous turbulence.

4. Discussion

The previous results have shown that three regions could be recognised in the flow. In fact it is possible, using LSS and the exponents ζ_p^{**} defined in equation (8) to follow continuously the radial evolution of the intermittency in the cell. The evolution of ζ_2^{**}, ζ_3^{**} and ζ_4^{**} as a function of r are plotted on Figure 16 a, b and c. In the outer region they have values close to those that are to be expected in normal turbulence (around 0.95 for ζ_2^{**}, ζ_3^{**} and ζ_4^{**}). In the central region they come closer to the value $\zeta_p^{**} = 1$ which corresponds to the perfect self similarity among the scales. In between there is a narrow range where the values are much smaller corresponding to enhanced intermittency.

Since the external part of the flow looks like usual turbulence and since the region neighbouring the vortex central region can be interpreted as a mixing of the "external turbulence" and the "vortex central region turbulence", the main points to be discussed are the properties of the velocity signal in the vortex central region.

The first feature in this region is the low level of fluctuations. The main remaining fluctuation is somewhat periodic and corresponds to the large peak observed at small wave number in the spectrum (*Fig.* 8). It is due to the slow motion of the vortex, also observed in the experiment using water. As shown by a comparison of Figure 4c and 8 all the other fluctuations are reduced, the large scale ones by a factor around 10. Furthermore, the intermittency inside the vortex core is also stronly reduced: the velocity increments PDFs no longer exhibit

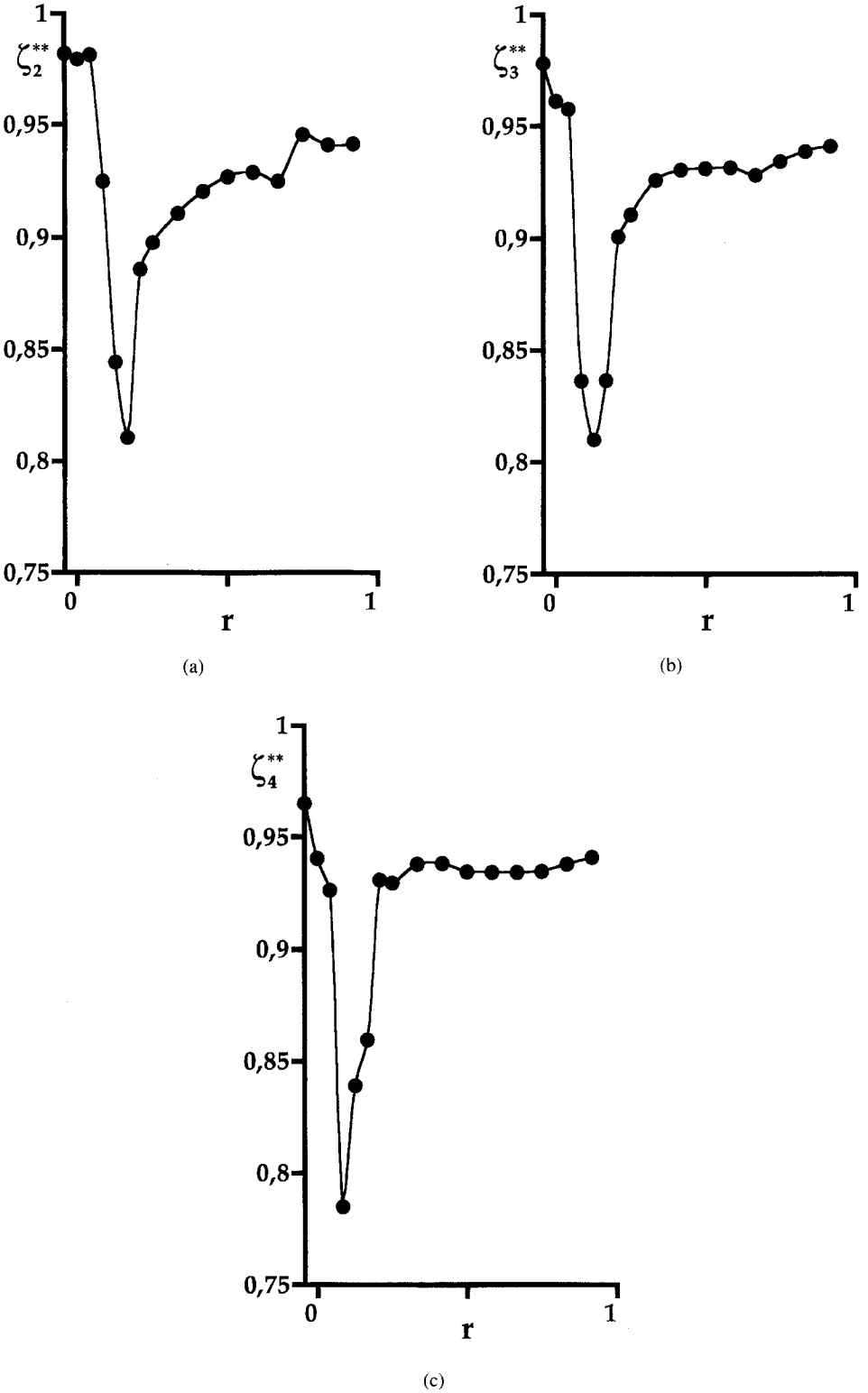

Fig. 16. – Spatial evolution of the values of the exponents ζ_p^{**} obtained by the variant LSS of ESS (see text). (a) ζ_2^{**} (b) ζ_3^{**} (c) ζ_4^{**}.

stretched tails and are more self-similar from scale to scale. Quantitatively the striking point is that the energy spectrum has a well defined but weaker slope (increasing from – 1.25 to – 1.05 inwards), and that the scaling exponents are smaller than usual. There are thus relatively more "small scales" in the signal than usual.

At least two effects can contribute to a reduction of the fluctuations, the small scales being less affected than the large ones. One is rather of dynamical nature while the other is more kinematical.

The main characteristic of a large Reynolds number vortex is its rotation. It is well known that in a fluid system the rotation has a bidimensionalising effect and that three-dimensional fluctuations are radiated by inertial waves. Even though in the case of a vortex, the large scale flow differs from a solid body rotation, this effect should act to reduce the 3D velocity fluctuations. The importance of this effect on a given fluctuation can be characterised by the product of the local angular velocity by the typical fluctuation timescale. In the case of turbulence, the fluctuations at small scale have a much smaller characteristic time that at large scale. The effect of rotation will thus be more important for large scale fluctuations.

It is noteworthy however that the main features of the velocity signal obtained here are not those observed in 3D rotating turbulence (i.e. fluctuations superimposed to a strong solid body rotation) or in 2D turbulence. For instance, in these cases, the cascade exhibits a k^{-3} range. As shown by Jacquin *et al.* (1990), the decay of turbulence is slower in the presence of rotation. The dissipation rate of the turbulent kinematic energy is therefore lower compared to non rotating conditions. For a constant forcing, this effect induces an increase of the total energy and thus of the fluctuation rate (inverse energy cascade, see Hossain (1993)). In the vortex flow investigated here, the lower dissipation in the vortex central region is observed but together with a decrease of the fluctuations. This difference may come from the inhomogeneity of the rotation in our experiment compared to the rotating turbulence. In particular, the large scale vortex continuously interacts with the fluctuating non-strongly rotating external turbulence.

The second mechanism which can be evoked is linked with the topology of the streamlines around the vortex. These streamlines are nearly closed or at least wrapped around the vortex. This has a first effect which is to protect the vortex from external perturbations. Moreover, the differential rotation around the vortex core induces a "sheetisation" of any structure in this region. An initial large scale perturbation is thus stretched by the strain rate field of the vortex and becomes thinner and thinner. This differential advection is thus also a mechanism of production of small scales.

Finally it can be noted that the observed energy spectrum could simply correspond to a signal composed of localised events having a large band signature. If we consider a signal composed of independent peaks, the corresponding energy spectrum has a k^{-1} range. Indeed, an isolated singularity is the simplest self-similar signal. This could be coherent with what is observed in the time series of the signal which has the best k^{-1} spectrum. In this case some isolated peaks decorate the large scale fluctuating signal which corresponds to the vortex vibration. Their typical size is of the order of the small scale cut-off of the power spectrum, and their mean separation corresponds to the wavenumber at which this k^{-1} scaling starts. This is for instance the interpretation given by Jimenez *et al.* (1993) for the tendency to an energy spectrum in k^{-1} in the region of large vorticity (the so-called worms). It is also related to the observation by Townsend (1951) that a random array of point vortices exhibits such a k^{-1} range in the energy spectrum.

5. Conclusion

A large Reynolds number vortex was generated in low temperature Helium gas. This vortex was stretched, and thus stabilised, by pumping on its axis. The turbulent tangential velocity fluctuations were recorded for different positions of the probe. Far from the vortex, the large velocity fluctuations look roughly like those of

a turbulent boundary layer, at least for the statistical quantities computed here. The one-dimensional energy spectrum has a range in which it is close to the $k^{-5/3}$ behaviour and the scaling exponents usually obtained are approximately recovered. In contrast, in the vortex central region some drastic changes are observed. The fluctuations and the dissipation are reduced and the energy spectrum exhibits a smaller slope which tends towards k^{-1}. This may correspond to the presence of independent peaks in the velocity signal. Moreover, the central region tends to present a vanishing intermittency and the velocity increments distributions are close to being self-similar from scale to scale. It is in itself an interesting result that it is possible to find simple characteristics for such an anomalous turbulence. In the present case, even at a large Reynolds number, we did not find an indication of isotropisation of the small scales. This result clearly indicates a coupling between small and large scales in the vicinity of a turbulent vortex. The local anisotropy of fine-scale structures under the influence of a vortex was observed by Melander and Hussain (1993) in a moderate Reynolds number simulation. Investigating experimentally the turbulent flow generated by two corotating disks (but without stretching), Pinton and Dernoncourt (1997) also found energy spectra which exhibit well defined "inertial ranges" with anomalous slopes (from – 2 to – 1 depending on the situation). Their results may also be interpreted as due to the influence of the large scale rotation.

The next question is whether or not these results have any relevance to the understanding of a normal turbulent flow. It is now well established that such a turbulent flow contains coherent vortex filaments. There is a direct signature, a *kinematic* one of the presence of these vortex filaments in a turbulent flow. It had been clearly identified in the time series of the velocity recording in the previous work of Cadot *et al.* (1994) and of Belin *et al.* (1996). The present work suggests that there may also be a *dynamical influence* of a coherent vortex on the surrounding turbulence. In particular, a large scale vortical structure could have, on the neighbouring small scale fluctuations, a large enough influence to modify the local spectrum and the intermittency. More work is still needed because there may be large differences between the forced stable vortex which has little freedom of evolution, and the spontaneously formed vortices which are embedded in a turbulent flow.

Acknowledgements. – We thank F. Belin and H. Willaime for their help in the signal processing, P. Tabeling for hosting us, and all for very useful discussions. This work benefited from the support of CNRS (France) and DRET (Contract No. 95-111/DRET).

REFERENCES

ANDREOTTI B., DOUADY S., COUDER Y., 1997, About the interaction between vorticity and stretching, in *Turbulence modelling and vortex dynamics*, edited by O. BORATAV, A. EDEN and A. ERZAN, Lecture Notes in Physics, Springer, p. 92-107.

ANDREOTTI B., DOUADY S., 1997, A regularisation method to improve the estimate of a probability distribution function from an experimental histogram, Preprint.

ARNEODO A. et al., 1996, Structure functions in turbulence, in various flow configurations, at Reynolds number between 30 and 5000 using extended self similarity, *Europhys. Lett.*, **34**, 411-416.

BELIN F., MAURER J., TABELING P., WILLAIME H., 1996, Observation of intense filaments in fully developed Turbulence, *J. Phys. II France*, **6**, 573-583.

BENZI R., CILIBERTO S., BAUDET C., TRIPICCIONE R., MASSAIOLI F., SUCCI S., 1993, Extended self-similarity in turbulent flows, *Phys. Rev. E.*, **48**, R 29.

BURGERS J. M., 1940, Application of a model system to illustrate some points of the statistical theory of free turbulence, *Proc. Acad. Sci. Amsterdam*, **43**, 2-12.

CADOT O., DOUADY S., COUDER Y., 1994, Characterisation of the low-pressure filaments in a three dimensional turbulent shear flow, *Phys. Fluids*, **7**, 1-15.

CASTAING B., CHABAUD B., HEBRAL B., 1992, Hot wire anemometer operating at cryogenic temperatures, *Rev. Sci. Instrum.*, **63**, 4167-4173.

CHILLA F., PINTON J. F., LABBE R., 1996, On the influence of a large scale coherent vortex on the turbulent cascade, *Europhys. Lett.*, **35**, 271-276.

DUBRULLE B., 1994, Intermittency in fully developed Turbulence: Log-Poisson statistics and generalised scale covariance, *Phys. Rev. Lett.*, **73**, 959-962.

ESCUDIER M. P., 1984, Observations of the flow produced in a cylindrical container by a rotating endwall, *Exp. Fluids*, **2**, 189-196.

HOPFINGER E. J., BROWAND F. K., GAGNE Y., 1982, Turbulence and waves in a rotating tank, *J. Fluid Mech.*, **125**, 505-534.

HOSSAIN M., 1993, Reduction in the dimensionality due to strong rotation, *Phys. Fluids*, **6**, 1077-1080.

JACQUIN L., LEUCHTER O., CAMBON C., MATHIEU J., 1990, Homogeneous turbulence in the presence of rotation, *J. Fluid Mech.*, **220**, 1-52.

JIMENEZ J., WRAY A. A., SAFFMAN P. G., ROGALLO R. S., 1993, The structure of intense vorticity in isotropic turbulence, *J. Fluid Mech.*, **255**, 65-90.

LABBE R., PINTON J. F., FAUVE S., 1996, Study of the von Karman flow between coaxial corotating disks, *Phys. Fluids*, **8**, 914-922.

MAURER J., TABELING P., ZOCCHI G., 1994, Statistics of turbulence between two counterrotating disks in low temperature helium gas, *Europhys. Lett.*, **26**, 31-36.

MELANDER M. V., HUSSAIN F., 1993, Coupling between a coherent structure and fine scale turbulence, *Phys. Rev. E*, **48**, 2669-2689

MOORE D. W., SAFFMAN P. G., 1972, The motion of a vortex filament with axial flow, *Phil. Trans. R. Soc. Lond.*, **272**, 403-429.

MORY M., SPOHN A., 1992, Vortex Flow generated by a rotating disk, in *Rotating Fluids in geophysical and industrial applications*, edited by E. HOPFINGER, Springer Verlag.

PINTON J. F., LABBE R., 1984, Correction to the Taylor hypothesis in swirling flows, *J. Phys. France*, **4**, 1461-1468.

PINTON J. F., DERNONCOURT B., 1997, On the influence of vorticity filaments on small scale intermittency, this issue of *Eur. J. Mech. B Fluids*.

SADDOUGHI S., VEERAVALLI S. V., 1994, Local isotropy in turbulent boundary layers at high Reynolds number, *J. Fluid Mech.*, **268**, 333-372.

SAFFMAN P. G., 1968, Lectures on Homogeneous Turbulence, in *Topics in Nonlinear Physics*, edited by N. J. ZABUSKY, Springer-Verlag.

SHE Z.-S., LÉVÊQUE E., 1994, Universal scaling laws in fully developed turbulence, *Phys. Rev. Lett.*, **72**, 336-340.

TANAKA M., KIDA S., 1993, Characterization of vortex tubes and sheets, *Phys. Fluids A*, **5**, 2079-2082.

TOWNSEND A.A., 1951, ON the fine scale structure of turbulence, *Proc. R. Soc. Lond. A*, **208**, 534-542.

TSINOBER A., KIT E., DRACOS T., 1992, Experimental investigation of the field of velocity gradients in turbulent flows, *J. Fluid Mech.*, **242**, 169-192.

TURNER J. S., 1996, The constraints imposed on tornado-like vortices by the top and bottom boundary conditions, *J. Fluid Mech.*, **25**, 377-400.

ZOCCHI G., TABELING P., MAURER J., WILLAIME H., 1994, Measurement of the scaling of the dissipation at high Reynolds numbers, *Phys. Rev. E*, **50**, 3693-3700.

(Received 01 August 1997,
revised and accepted 20 November 1997)